THE ASTROPHYSICAL JOURNAL, 541:1096–1103, 2000 October 1

SCALING LAWS FOR A NANOFLARE-HEATED SOLAR CORONA

G. VEKSTEIN[1] AND Y. KATSUKAWA[2]
Received 2000 February 22; accepted 2000 May 15

ABSTRACT

The concept that the solar corona is heated by numerous small flarelike events dubbed "nanoflares" is considered. The hot corona is viewed as an ensemble of high-temperature elemental magnetic filaments created within the coronal magnetic field by randomly distributed impulsive heating events. It is shown that such an approach allows us to predict various signatures of X-ray coronal loops without specifying the details of the heating process. In particular, the dependence of the temperature, filling factor, and emission measure on the length of the loop and strength of the coronal magnetic field is derived. The obtained scaling laws fit reasonably with observational data.
Subject headings: MHD — Sun: corona — Sun: flares

1. INTRODUCTION

Although it is generally accepted now that the mechanism responsible for maintaining high plasma temperature ($T > 10^6$ K) in the solar corona is intimately related to the coronal magnetic field, detailed understanding of the process is still far from completion. Moreover, it is likely that different heating mechanisms operate in various large-scale structures observable in the corona (loops, coronal holes, X-ray–bright points, etc.). As energy for coronal heating is ultimately tapped from the mechanical energy of the photospheric fluid motion, the problem is to explain how the latter affects the coronal magnetic field and, most crucially, how the resulting excess magnetic energy is converted into heat. Broadly, all theories of the magnetic coronal heating divide into two classes: wave models, if the timescale of the driving photospheric motions is fast compared with the Alfvén transit time in the coronal field, and quasi-static models, if the driving time is slow (see, e.g., Ulmschneider, Rosner, & Priest 1991). In the latter case, relevant for active regions with bipolar magnetic geometry and relatively strong magnetic field, continuous shuffling of photospheric footpoints makes the coronal field evolve through a series of magnetostatic equilibria. Thus, in a low-beta corona the magnetic field remains almost force free, with field-aligned electric currents as a source of the excess magnetic energy available for plasma heating.

However, the electric conductivity of hot coronal plasma is so high, and hence the resulting Ohmic dissipation rate, derived on global length scales, so small, that such conventional conversion of the magnetic energy into heat becomes completely irrelevant. Therefore, for magnetic heating to be effective, fine-scale magnetic structures, known as current sheets, must develop within the coronal magnetic field in response to its external (photospheric) deformation (Parker 1972). Inside the current sheet even small plasma resistivity initiates magnetic reconnection, which breaks the field topology conservation constraint of the ideal magnetohydrodynamics and, hence, allows fast transition of the coronal configuration to a state of lower magnetic energy (see, e.g., Priest 1982). Moreover, this process can be facilitated even further by the anomalous plasma resistivity triggered inside the current sheet when electric current density there exceeds a certain threshold (Galeev & Sagdeev 1984). It is well understood now that current sheets are likely to be ubiquitous in the corona because of its usually complex magnetic structure as well as the chaotic nature of the turbulent photospheric motions (Low & Wolfson 1988; Van Ballegooijen 1988; Vekstein, Priest, & Amari 1991). Thus, the process of magnetic coronal heating is likely to be highly fragmented, both in space and time, and hence can be viewed as an integral effect of numerous small-scale energy release events dubbed "nanoflares" (Parker 1988). This concept bridges two historically separate solar physics research areas, flares and coronal heating, considering nanoflares as the lower energy population of a broad spectrum of flarelike events.

Unfortunately, individual nanoflares cannot be resolved observationally, neither at present nor in the foreseeable future. Therefore, to test the nanoflare concept of coronal heating, one should turn to the statistical characteristics of active regions, which result presumably from a large number of more or less random heating events. Treating this problem from "first principles" of resistive magnetohydrodynamics is a formidable task even for numerical simulation, and it is almost impossible analytically. Thus, to get insight into coronal heating by nanoflares, simplified models have been used, where each heating and subsequent cooling event was described roughly in a zero-dimensional approximation (average along a magnetic loop), putting emphasis on the coronal response to many such events. Thus, Kopp & Poletto (1993) studied evolution of a single loop of fixed length and aspect ratio subjected to continuous heating by nanoflares. Alternatively, Cargill (1994) considered a large number (many thousands) of elementary loops (filaments) heated by sporadic energy depositions, aiming to obtain the filling factor (proportion of hot filaments) for such an ensemble, as well as the temperature distribution of these filaments and the differential emission measure of the system. However, all these characteristics essentially depend on the cross-sectional area of an individual filament, which in the above papers has been imposed more or less arbitrarily. Therefore, the best that can be achieved with this approach is simply to match observations by varying the filament size or, equivalently, the total number of elemental filaments within an observed bright coronal loop (Cargill & Klimchuk 1997).

[1] Department of Physics, University of Manchester Institute of Science and Technology, Manchester, M60 1QD, England, UK.
[2] Department of Astronomy, School of Science, University of Tokyo, Bunkyo-ku, Tokyo 113-0033, Japan.

We argue that from the point of view of the physics involved it is senseless to define such elemental filaments independently of the heating process, simply because they do not exist prior to the occurrence of the heating event. Thus, in the present paper we suggest a self-consistent definition of hot magnetic filaments created by nanoflares. The basic point is that primary energy dissipation, presumably via magnetic reconnection, occurs in a very narrow current sheet, with its width determined by the plasma resistivity (e.g., Vekstein & Jain 1999). Therefore, the released thermal energy, while spreading fast along the magnetic field, cannot remain localized across the field because of the otherwise very high thermal pressure there. Hence, hot plasma will expand across field lines until gas kinetic pressure inside the filament becomes equal to the external magnetic pressure, and this pressure balance requirement determines the cross-sectional area of the filament. Thus, the geometry of the coronal magnetic field shapes the lengths of filaments and, hence, of the loop as a whole, while the field strength and the amount of heat input define the diameter of hot filaments. Therefore, a broad energy spectrum of heating events (nanoflares) creates an ensemble of filaments with various sizes. This simple assumption enables us to derive observable integral characteristics of coronal loops without specifying particular details of the heating process that is behind their very existence.

The paper is organized as follows. Formation of a hot filament by an instant heating event and its subsequent thermal evolution are discussed in § 2. Integral parameters of bright loops (filling factor, temperature, and emission measure) viewed as a superposition of many hot filaments are derived in § 3. In § 4 we present a numerical simulation of nanoflare-heated X-ray loops. A summary of the obtained results, followed by a brief discussion, is drawn in § 5.

2. HOT FILAMENTS: CREATION AND THERMAL EVOLUTION

It is likely that the energy release process responsible for coronal heating, either magnetic reconnection or another one such as resonant wave absorption, is very fast compared with the typical lifetime of hot filaments. Therefore, in studying their thermal evolution one can assume the heating event as an instant deposition of some energy ΔW. As for the spatial scale of heating, the primary dissipation of the magnetic energy occurs inside a very thin current sheet. Its width is determined by plasma resistivity and might be extremely small in a plasma with a large magnetic Reynolds number such as the coronal plasma. Therefore, the released thermal energy cannot remain localized inside the current sheet but will spread along the magnetic field and expand across it until thermal pressure of the hot plasma comes into equilibrium with the external magnetic pressure. Assuming fast thermalization of the released energy, the filament becomes filled with a plasma of density n_0 and temperature T_0, so the above-stated pressure balance requirement is

$$2n_0 kT_0 = B^2/8\pi \ , \tag{1}$$

where B is the magnitude of the coronal magnetic field. Of course, a general pressure balance equation should include both the thermal and magnetic pressures inside and outside the filament. However, hot plasma expands together with the frozen-in magnetic field. This results in a substantial reduction in the magnetic field inside the filament; hence it becomes much weaker than the outside field (initially both fields are the same). As the filling factors of active region loops are likely to be small (see below), each new hot filament is formed within an initially "empty" coronal magnetic field where the plasma pressure is negligibly small. That is why the thermal pressure is omitted in the right-hand side of equation (1). For the same reason the pre-event thermal energy of the filament is also small, so the energy conservation condition, which takes into account the energy of expansion, is

$$\Delta W = 5n_0 kT_0 L \Delta S \ , \tag{2}$$

where L is the length of the filament and ΔS its cross-sectional area, yielding

$$\Delta S = \frac{16\pi}{5} \times \frac{\Delta W}{B^2 L} \ . \tag{3}$$

Two points are worth noting here. First, the nanoflare energy ΔW has nothing to do with free magnetic energy stored within the volume of the hot filament given by equation (3) or with that inside a current sheet where initial dissipation occurs. Instead, the above energy is associated with the global excess energy of a system (Vekstein & Jain 1998), which is brought into the dissipation region by Poynting flux during the reconnection process. Second, expression (3) should be viewed not as a strict relation but more as a rough estimate of a minimum size of the heated filament. This is because the coronal magnetic field is nonuniform and also because of the possible instability of a plasma–magnetic field boundary, which might increase the filament size. As an illustrative example, a nanoflare with energy $\Delta W = 10^{24}$ ergs creates, according to equation (3), a hot filament with diameter $d \approx 4 \times 10^6$ cm for $B = 30$ G and $L = 10^9$ cm.

As seen from equation (1), the initial temperature of the filament, T_0, might be quite high when the density n_0 is low. For example, if $B = 30$ G, $T_0(\mathrm{K}) = 1.3 \times 10^{17}/n_0$, giving $T_0 > 10^8$ K for $n \lesssim 10^9$ cm^{-3}. Therefore, thermal evolution of the coronal filament at this stage is determined by interaction of its strong heat flux with the lower lying dense chromosphere. Such interaction involves complicated time-dependent supersonic flows and shock waves and thus hardly can be treated analytically. However, description of the filament cooling becomes substantially simplified when the temperature falls and chromospheric evaporation upflow becomes subsonic. The respective criterion (Antiochos & Sturrock 1978) is

$$\frac{T^2}{nL} \lesssim 3 \times 10^{-5} \ . \tag{4}$$

Assuming that the total thermal energy in the filament remains unchanged, so does the plasma pressure $2nkT = B^2/8\pi$; the onset of subsonic chromospheric evaporation occurs when

$$T \approx T_1 \approx 2 \times 10^3 B^{2/3} L^{1/3} \ , \quad n \approx n_1 \approx 7 \times 10^{10} B^{4/3} L^{-1/3} \ , \tag{5}$$

and it translates into $T_1 \approx 2 \times 10^7$ K and $n_1 \approx 6.5 \times 10^9$ cm^{-3} for $B = 30$ G and $L = 10^9$ cm. Then simple order-of-magnitude estimates of the characteristic timescales for the filament cooling by heat conduction (τ_c) and radiation (τ_r)

read (e.g., Cargill 1993)

$$\tau_c = \frac{4 \times 10^{-10} n L^2}{T^{5/2}} \text{ (s)} , \quad \tau_r = \frac{2 \times 10^3 T^{3/2}}{n} \text{ (s)} . \tag{6}$$

At the temperature T_1 and density n_1 given by equation (5) estimates (6) yield

$$\tau_{c1} \approx 1.6 \times 10^{-7} L^{5/6} B^{-1/3} , \quad \tau_{r1} \approx 2.6 \times 10^{-3} L^{5/6} B^{-1/3} . \tag{7}$$

As seen from equation (7), $\tau_{c1} \ll \tau_{r1}$, so the filament cooling can be viewed as a two-stage process (Cargill 1993). During the first, conductive stage, radiation losses can be neglected and the total thermal energy in the filament is conserved as the downward conductive heat flux is balanced by the evaporative upflow of enthalpy. Then the temperature of the filament is decreasing and its density increasing as follows (Antiochos & Sturrock 1978):

$$T(t) = T_1(1 + t/\tau_{c1})^{-2/7} , \quad n(t) = n_1(1 + t/\tau_{c1})^{2/7} . \tag{8}$$

Such evolution continues until the two cooling times defined in equation (6) become equal at

$$t = t_* \approx \tau_{c1}(\tau_{r1}/\tau_{c1})^{7/12} \approx 3 \times 10^2 \tau_{c1} , \tag{9}$$

when the temperature falls to

$$T = T_* = T_1(\tau_{c1}/\tau_{r1})^{1/6} \approx 4 \times 10^2 B^{2/3} L^{1/3} \tag{10}$$

while density reaches its maximum

$$n = n_* \approx 3.5 \times 10^{11} B^{4/3} L^{-1/3} . \tag{11}$$

As an illustration for these temperatures T_* and densities n_*, which are important in shaping integral characteristics of coronal loops (see § 3), for $B = 30$ G and $L = 10^9$ cm expressions (10) and (11) yield $T_* \approx 4 \times 10^6$ K and $n_* \approx 3.2 \times 10^{10}$ cm^{-3}.

The subsequent cooling of the filament is governed mainly by radiation losses. The precise behavior of the temperature at this stage depends on how fast the coronal material is drained out of the filament (Serio et al. 1991; Cargill, Mariska, & Antiochos 1995). Numerical simulations show that $n \propto T^{1/2}$ is a good approximation, so by adopting it one can then derive from equation (6) that $T \approx T_*(1 - t/t_*)$. Thus, it takes the radiation time interval $(\Delta t)_r \sim t_*$ to cool a filament to such a low temperature that all its material is evacuated by gravity; hence the filament ceases to exist. It is worth noting that $(\Delta t)_r$ is not very sensitive to details of the plasma drain, as it remains of the same order of magnitude as t_*. Therefore, the total lifetime $(\Delta t)_h$ of a hot filament created by a nanoflare can be estimated as

$$(\Delta t)_h = (\Delta t)_c + (\Delta t)_r \approx 2t_* \approx 10^{-4} L^{5/6} B^{-1/3} . \tag{12}$$

For the coronal parameters used above, namely, $B = 30$ G and $L = 10^9$ cm, it results in $(\Delta t)_h \approx 10^3$ s.

The fact that both cooling stages have about the same duration equal to t_* is not a coincidence but follows from expressions (6) for their respective timescales. As the conductive time $\tau_c \propto n/T^{5/2}$, it is increasing while cooling. Thus, the total duration of the conductive stage, when the temperature falls from $T = T_1$ to $T = T_*$, is mainly determined by its final phase with $T \sim T_*$, so $(\Delta t)_c \sim \tau_c(T_*) \sim t_*$. On the other hand, the radiation time $\tau_r \propto T^{3/2}/n$ is decreasing while temperature falls; therefore $(\Delta t)_r$ is specified by the initial phase of radiation cooling resulting in $(\Delta t)_r \sim \tau_r(T_*) \sim t_*$.

This feature of the cooling of coronal filaments has important observational implications (see § 3) since during its lifetime $(\Delta t)_h$ a hot coronal filament is most likely to be in a state with temperature $T \sim T_*$.

3. FILLING FACTOR AND INTEGRAL CHARACTERISTICS OF CORONAL LOOPS

Knowing the thermal evolution of an individual hot filament, it is possible to derive observable characteristics of coronal loops by viewing the latter as superpositions of a large number of filaments. Let us start with an important diagnostic quantity known as the filling factor (f), i.e., the fraction of the total volume of the loop filled with hot X-ray–emitting plasma. Assuming that the heat flux q, which maintains a steady hot corona ($q \sim 10^7$ ergs cm^{-2} s^{-1} for active regions), is provided by elementary energy releases (nanoflares), each of which with energy ΔW, the occurrence rate of nanoflares per unit area is $q/\Delta W$. Thus, if a coronal loop has cross-sectional area S, there are, on average, $\dot{N} = 2Sq/\Delta W$ nanoflares occurring inside the loop per unit time (the factor of 2 is due to the two photospheric bases of the loop). As each nanoflare creates a hot filament with lifetime $(\Delta t)_h$ given by equation (12), the total number of such filaments present within the loop at any given time is

$$N = \dot{N}(\Delta t)_h = 2S \times \frac{q}{\Delta W} \times 10^{-4} L^{5/6} B^{-1/3} . \tag{13}$$

For example, if $B = 30$ G, $L = 10^9$ cm, $q = 10^7$ ergs cm^{-2} s^{-1}, $S = 10^{18}$ cm^2, and $\Delta W = 10^{24}$ ergs, there are $N \approx 2 \times 10^4$ filaments inside such a loop. Recalling the cross-sectional area of each filament given by equation (3), the filling factor of the loop can be estimated as (Vekstein 1996)

$$f = N \frac{\Delta S}{S} \approx 2 \times 10^{-3} q B^{-7/3} L^{-1/6} . \tag{14}$$

It follows from equations (13) and (14) that, although the total number of filaments inside the loop, N, depends on the nanoflare energy ΔW, the filling factor, f, does not; thus, expression (14) provides quite a universal theoretical prediction for the coronal filling factor. It shows that small values of f are likely to be expected, typically of the order of 10^{-1}–10^{-2} for the magnetic field $B \approx 30$–100 G and energy flux $q \approx 10^6$–10^7 ergs cm^{-2} s^{-1}. This conclusion is supported by several independent estimates of the coronal filling factor obtained from analysis of observational data (Cargill & Klimchuk 1997; Moore et al. 1999).

For the above model the filling factor can be also viewed from a different perspective by considering integral thermal characteristics of the loop. Introducing the plasma parameter β, which is the ratio of the thermal pressure, p_T, to the magnetic pressure $p_M = B^2/8\pi$, one finds that $\beta \sim 1$ inside hot filaments while $\beta \approx 0$ outside them. Thus, the average value of β is simply equal to the filling factor; i.e., $\langle \beta \rangle \approx f$. Then the total thermal energy of the loop, $W_T = (3/2)p_T V$, can be written as

$$W_T = \frac{3}{2} \frac{B^2}{8\pi} f L S \approx 10^{-4} q L^{5/6} d^2 B^{-1/3} , \tag{15}$$

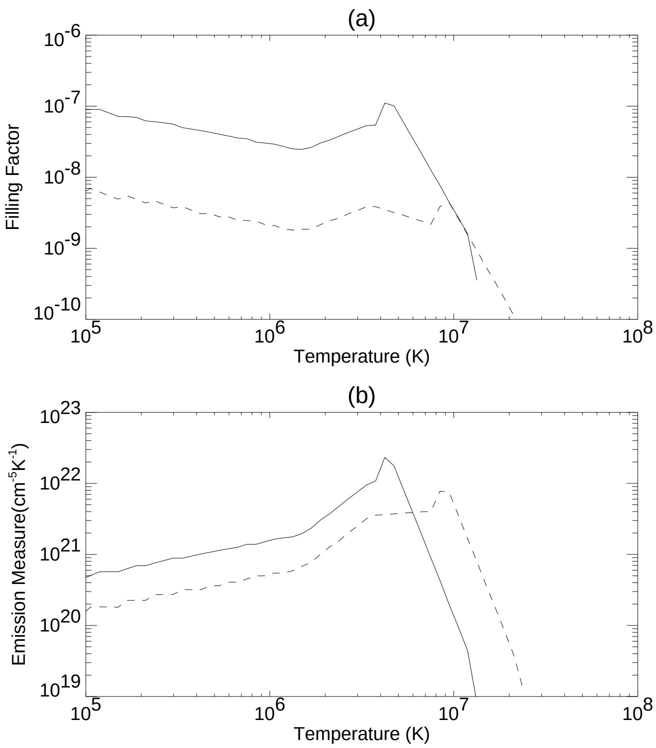

FIG. 1.—(*a*) Temperature distribution (differential filling factor) and (*b*) emission measure distribution for Loop 1. In both panels, the solid lines correspond to $B = 20$ G and the dashed lines to $B = 50$ G.

where d is the diameter of the loop. If coronal heating is provided by magnetic reconnection, it is reasonable to assume that the energy flux into the corona, q, is proportional to B^2. In this case both the total thermal energy and average pressure scale as W_T, $p_T \propto B^{5/3}$, a relation that is close to the well-known scaling $\propto B^{1.6}$ obtained from observational data (Golub et al. 1980).

Let us now consider such observational signatures of coronal loops as temperature and emission measure. As numerous hot filaments within a loop are at different phases of cooling, their distribution with temperature is quite broad and can be derived only by numerical simulation (see § 4). However, some important characteristics of the loop are not sensitive to the details of the above distribution but follow from basic features of the filament cooling described in the previous section. First, as the rate of heat loss has a minimum when transition from conductive to radiation cooling occurs, the respective cooling time is the longest at this moment; hence, while cooling, the hot filament spends most of its lifetime at this phase. Therefore, distribution of hot filaments with temperature peaks at the transition temperature $T \sim T_*$ given by equation (10) as seen from Figure 1*a*, where the numerically derived distribution of filaments is plotted. Furthermore, the density of the filament has a maximum at this temperature; thus, the distribution of the emission measure with temperature is concentrated at $T \approx T_*$ even more strongly than that for the filling factor (see Fig. 1*b*). If such a loop is observed with a broadband X-ray telescope, the detected loop temperature T_L should therefore be close to T_*, so the model predicts the following expression for T_L:

$$T_L \approx 4 \times 10^2 B^{2/3} L^{1/3} . \qquad (16)$$

As this scaling originates from the requirement that conduction and radiation losses are approximately equal, expression (16) is formally equivalent to the well-known Rosner-Tucker-Vaiana (RTV) relation (Rosner, Tucker, & Vaiana 1978) if the plasma pressure there is put equal to the magnetic pressure. Its physical meaning is, however, quite different. In our context equation (16) applies not to a steady state thermal equilibrium of a single loop as the RTV relation does but to the statistical steady state of the complex loop comprising a large number of filaments, each of which is inherently time dependent.

The total emission measure, $(\mathrm{EM})_t$, of a bright coronal loop can also be estimated by exploring the above-mentioned sharp maximum in its differential temperature distribution. As the plasma density n_* that corresponds to the transition temperature T_* is given by equation (11), the total emission measure, according to equations (11) and (14), is equal to

$$(\mathrm{EM})_t \approx n_*^2\, fV \approx 2 \times 10^{20} q B^{1/3} d^2 L^{1/6} . \qquad (17)$$

Taken together, equations (11) and (14)–(17) provide scaling laws for a nanoflare-heated corona. They can be used for estimating the coronal magnetic fields and filling factors of X-ray loops by comparing these theoretical predictions with observational data. For this purpose we explore here the same set of five active region loops observed by the *Yohkoh* Soft X-ray Telescope (SXT) as was selected by Cargill & Klimchuk (1997). The procedure is as follows. The observed temperature, T_L, and half-length, L, of the loop are used in equation (16) to obtain the magnetic field, B. By knowing the latter, as well as the observed total emission measure, $(\mathrm{EM})_t$, and the loop diameter, d, one can use equation (17) to derive the energy flux, q, required to provide the observed

TABLE 1

ACTIVE REGION LOOPS OBSERVED BY *Yohkoh* SXT

Parameter (1)	Loop 1 (2)	Loop 2 (3)	Loop 3 (4)	Loop 4 (5)	Loop 5 (6)
$L(10^9$ cm)[a]	3.82	4.53	3.08	3.20	8.16
$d(10^9$ [a]	1.48	1.15	1.55	2.12	1.45
$T(10^6$ K)[a]	6.39	4.47	7.25	1.88	2.05
$(\mathrm{EM})_t(10^{46}$ cm^{-3})[a]	21	7.7	0.25	7.5	240
B(G)[b]	33	18	44	5.8	4.1
$q(10^6$ ergs cm^{-2} s^{-1})[b]	3.8	2.7	0.04	1.2	80
f[b]	5.6×10^{-2}	1.6×10^{-1}	3.1×10^{-4}	≈ 1	>1

[a] Observed parameters.
[b] Those derived from scaling laws (eqs. [14]–[17]).

emission. Then the filling factor, f, follows from equation (14). The result is shown in Table 1, where both observed and theoretically derived parameters of each loop are shown.

It is seen that loops 1–3 fit well into the suggested nanoflare heating model with a small filling factor, thus confirming the earlier conclusion of Cargill & Klimchuk (1997). Particular values of the filling factor for these loops derived from the scaling law (14) are also very close to those obtained in the above-mentioned paper by using an extensive numerical simulation. As seen from Table 1, though loop 4 with its filling factor $f \approx 1$ probably just fits into the model, loop 5 definitely does not, as the filament density n_* given by equation (11) ($n_* \approx 10^9$ cm^{-3} in this case) falls short of explaining the large detected emission measure. Although the cause of this anomaly is not yet clear (see discussion in Cargill & Klimchuk 1997), one might speculate that it is somehow related to the extremely weak magnetic field of this loop as shown in Table 1. As for the magnetic fields in the "normal" loops 1–3, the above given values look quite reasonable, especially after accounting for the fact that these are actually field estimates from below because the plasma parameter β in elemental hot filaments might well be less than unity (see § 2).

4. NUMERICAL SIMULATION

Here we present the results of the numerical simulation of the nanoflare coronal heating for the model described above. The aim is to demonstrate in detail internal composition of bright coronal loops, thus providing quantitative support to basic conclusions and scaling laws drawn in §§ 2–3.

We assume that energy distribution of nanoflares has a simple power-law spectrum; i.e., it is proportional to $(\Delta W)^{-\alpha}$ and bounded between some minimum and maximum energy releases, $(\Delta W)_{\min}$ and $(\Delta W)_{\max}$, respectively. As a result of the very idea of the nanoflare heating scenario, namely, that coronal energy balance is maintained by small-scale energy release events, the power-law index α should be greater than 2. Then, if $(\Delta W)_{\max} \gg (\Delta W)_{\min}$, the occurrence rate of nanoflares per unit energy interval can be written in terms of the average energy flux q as

$$\frac{d(\Delta \dot{N})}{d(\Delta W)} = \frac{q(\alpha - 2)}{(\Delta W)^2_{\min}} [\Delta W/(\Delta W)_{\min}]^{-\alpha} . \quad (18)$$

It follows from equation (18) that the average number of nanoflares per unit area per unit time is

$$\langle \dot{N} \rangle = \int_{(\Delta W)_{\min}}^{(\Delta W)_{\max}} \frac{d(\Delta \dot{N})}{d(\Delta W)} d(\Delta W) = \frac{q}{(\Delta W)_{\min}} \times \frac{\alpha - 2}{\alpha - 1} , \quad (19)$$

with the average energy of each of them equal to

$$\langle \Delta W \rangle = (\Delta W)_{\min}(\alpha - 1)/(\alpha - 2) . \quad (20)$$

Each nanoflare with energy ΔW creates a hot filament with cross-sectional area ΔS specified by equation (3), so ΔS varies between $(\Delta S)_{\min}$ and $(\Delta S)_{\max}$ in proportion to $(\Delta W)_{\min}$ and $(\Delta W)_{\max}$. Therefore, in order to resolve the smallest filaments with size $(\Delta S)_{\min}$, we divided the whole cross-sectional domain of the loop under simulation into small grids each of size $(\Delta S)_g = 0.1(\Delta S)_{\min}$. Then nanoflares are generated randomly inside these grids, with the occurrence rate per unit time equal, according to equations (19) and (20), to $q(\Delta S)_g/\langle \Delta W \rangle$. Once created by a nanoflare, the hot filament evolves according to the two-stage cooling scheme described in § 2, with the initial temperature and density given by equation (5). At the radiation stage we use the same radiation loss function as Cargill & Klimchuk (1997), that is,

$$P_r = \begin{Bmatrix} 3.46 \times 10^{-25} T^{1/3} , & T > 10^{6.55} \\ 3.53 \times 10^{-13} T^{-3/2} , & 10^{6.18} < T < 10^{6.55} \\ 1.91 \times 10^{-22} , & T < 10^{6.18} \end{Bmatrix} , \quad (21)$$

and assume that plasma drain from the cooling filament scales as $n \propto T^{1/2}$.

As an example, we consider loop 1 of Cargill & Klimchuk (1997) using its observed parameters listed in Table 1. Since average integral characteristics of the loop, such as its temperature and emission measure, are not sensitive to parameters $(\Delta W)_{\min}$, $(\Delta W)_{\max}$, and α of the nanoflare spectrum, in this section we keep them fixed as follows: $\alpha = 3$, $(\Delta W)_{\min} = 3 \times 10^{23}$ ergs, and $(\Delta W)_{\max} = 3 \times 10^{26}$ ergs. Their effect on the variability of the loop, observed as X-ray and EUV brightenings (Shimizu 1995; Krucker & Benz 1998), is briefly discussed in § 5.

Simulation results are shown in Figures 1–3. The temperature distribution established in the loop (the differential filling factor) is plotted in Figure 1a for two different magnitudes of the coronal magnetic field (20 and 50 G). This distribution confirms general conclusions drawn in §§ 2–3 about the special role of the transition temperature T_* and

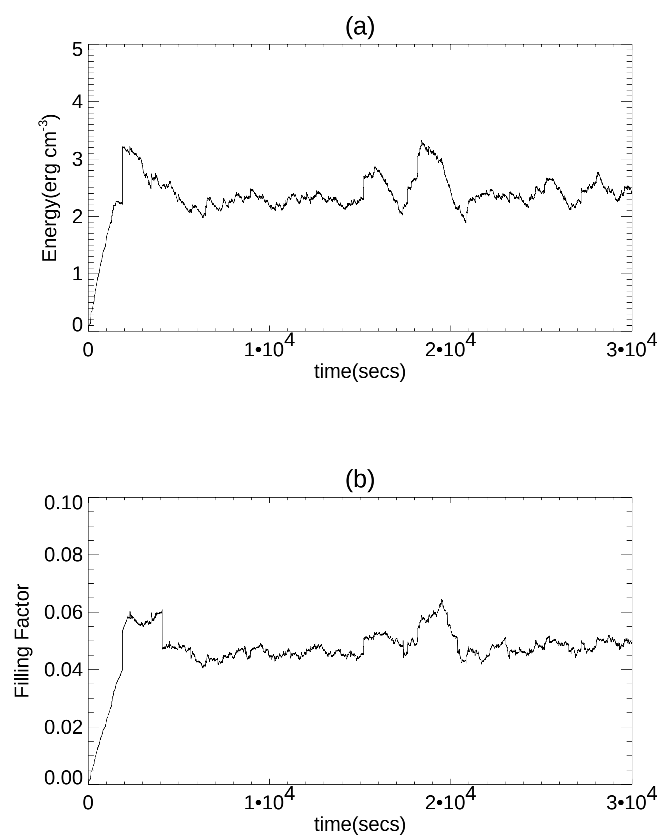

FIG. 2.—Time profiles of (a) thermal energy per unit volume and (b) filling factor as a result of the numerical simulation for Loop 1. The value of the magnetic field is 35 G.

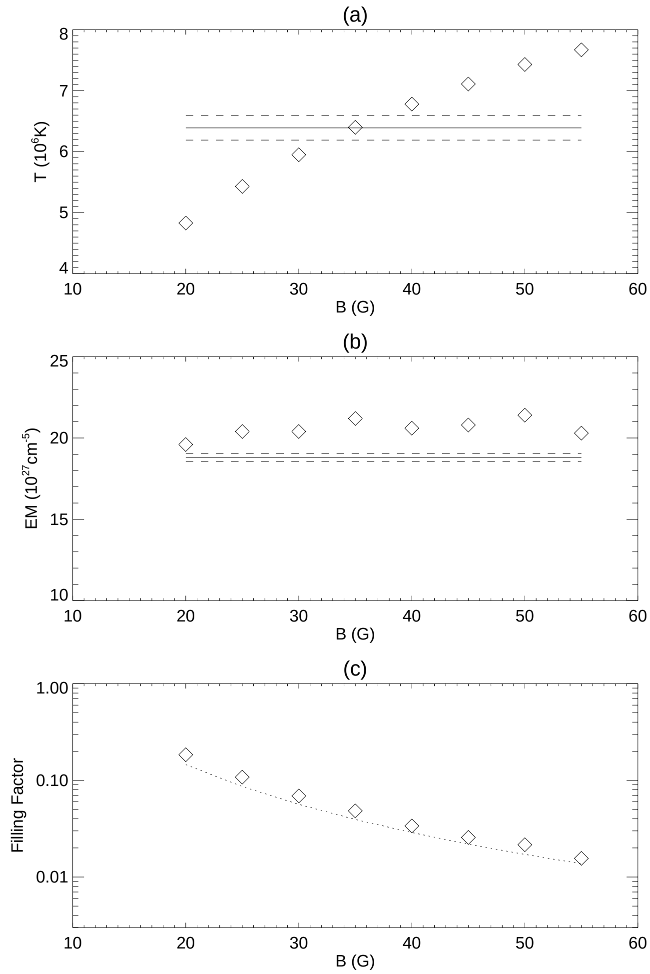

FIG. 3.—(*a*) Temperature, (*b*) emission measure, and (*c*) filling factor as a function of magnetic field for Loop 1. The diamonds represent the results of numerical simulations. In (*a*) and (*b*), the horizontal lines denote the quantities measured by SXT (*solid lines*) and their uncertainties (*dashed lines*). The dotted curve in (*c*) denotes the estimate of the filling factor given by eq. (14).

its scaling with the magnetic field (see eq. [10]). A similar distribution for the emission measure is shown in Figure 1*b*. The time history of the thermal energy in the loop, starting from the initial moment when the nanoflare generator is switched on and lasting for many characteristic cooling times until the statistical steady state is established, is plotted in Figure 2*a*. Figure 2*b* shows the evolution of the filling factor, which is defined here as the proportion of the loop volume filled with plasma of temperature $T > 10^5$ K.

Since the magnetic field B is the only free parameter in this simulation, its magnitude in the loop can be obtained by finding the best fit with observational data. To do so, for each value of B we generated numerically the hot loop comprising many hot filaments, with steady state characteristics similar to those shown in Figures 1 and 2. Then we convolve the calculated emission measure distribution with the temperature response functions of the two SXT filters. Using the filter ratio method, one can then derive the temperature and emission measure of the loop that would be detected by the SXT.

The results and their comparison with real observations are shown in Figure 3. It is seen from the temperature diagram (Fig. 3*a*) that the best fit occurs for $B \approx 35$ G, the value that is pretty close to that estimated from scaling laws (eqs. [14]–[17]) and shown in Table 1. As dependence of the emission measure on the magnetic field is much weaker (see eq. [17]), the corresponding comparison using the emission measure diagram of Figure 3*b* is less apparent. Finally, Figure 3*c* shows variation of the filling factor with the coronal magnetic field, obtained from numerical simulation. As seen, its simple estimate given by equation (14), which is also plotted there, has quite a good accuracy.

5. DISCUSSION

We have investigated various observational signatures of bright X-ray coronal loops, which are viewed as a superposition of a large number of hot filaments created by heating events (nanoflares) randomly distributed in space and in time. The essential difference between the model we use and previous studies of a nanoflare-heated corona (Kopp & Poletto 1993; Cargill 1993, 1994; Cargill & Klimchuk 1997) is in the very definition of elemental hot filaments. Instead of imposing their aspect ratio or cross-sectional area arbitrarily and independently of the heating process, we suggested the following self-consistent scenario for formation of hot filaments by nanoflares. Once excess magnetic energy in the corona has been dissipated inside a very thin reconnecting current sheet, the produced hot plasma expands across field lines until its initially huge thermal pressure becomes balanced by the magnetic pressure of the coronal field. Thus, the diameter of a hot filament, specified by equation (3), is determined by two factors: the amount of deposited thermal energy and the strength of the magnetic field. Combined with the two-stage description of the filament cooling (Cargill 1993, 1994), such an approach provides scaling laws (eqs. [14]–[17]) for the filling factor of the loop and its temperature, thermal energy, and emission measure. These scaling relations are of quite a universal character, as they do not depend on details of the energy distribution of nanoflares. The only parameter of the heating process involved in equations (14)–(17) is the average energy flux q, which is specified by the global energy balance requirements. As a testing field for the above scaling laws, we use the same set of active region loops observed by the *Yohkoh*/SXT instrument that has been analyzed in detail by Cargill & Klimchuk (1997). As seen from Table 1, our analytical predictions fit well with conclusions drawn in the latter paper by using an extensive numerical simulation. Moreover, we are also able to estimate magnetic field in these loops. The result is $B \sim (20–50)$ G for "normal" loops that fit into the nanoflare-heating scenario with a small filling factor. As for "anomalous" loops, the estimate yields $B \sim 5$ G, and this quite weak magnetic field is probably the cause of their unusual characteristics.

However, the above-mentioned universality of scaling laws for the average integral parameters of bright coronal loops also has a negative side, as relations (14)–(17) do not provide any insight into details of the nanoflare heating (e.g., spectral index α, $(\Delta W)_{\min}$, etc.). Therefore, to probe these characteristics one should look into the variability of a loop, of which the observational signatures are X-ray and EUV transient brightenings (Shimizu 1995; Shimizu & Tsuneta 1997; Krucker & Benz 1998; Parnell & Jupp 2000). To illustrate this point, the time history of the energy and filling factor of the loop, calculated by the numerical simulation of our model, are plotted in Figures 4 and 5 for two

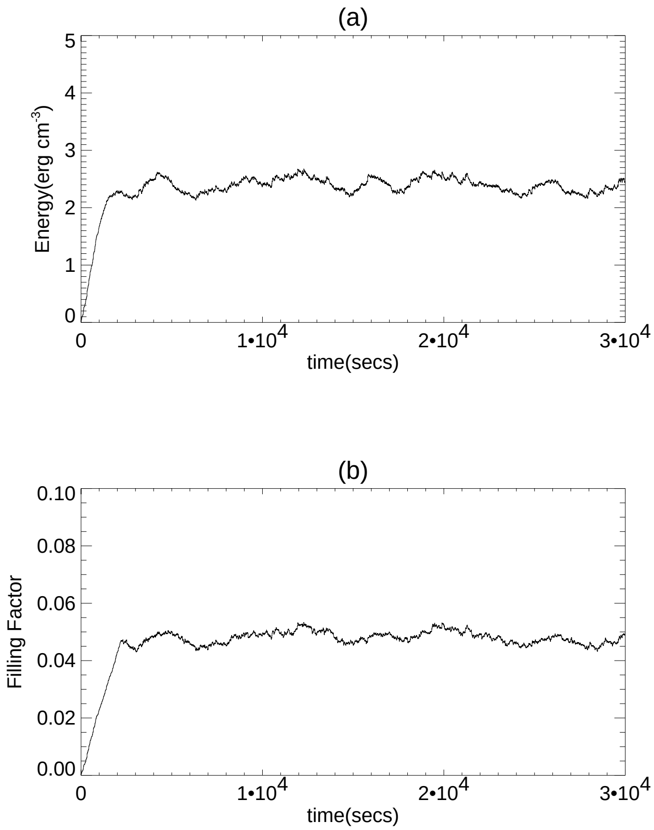

FIG. 4.—Time profiles of (*a*) thermal energy per unit volume and (*b*) filling factor for $\alpha = 4$. All other parameters are the same as in Fig. 2.

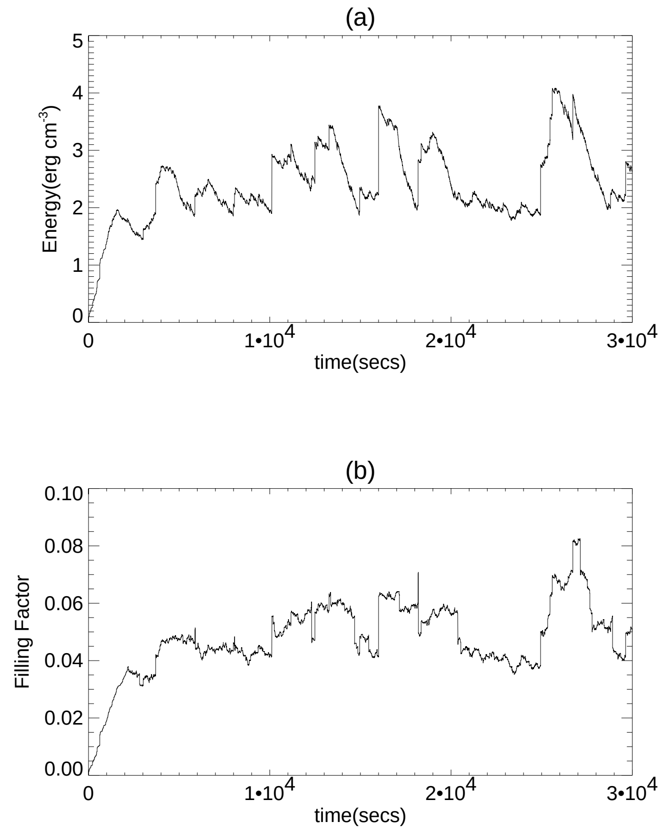

FIG. 5.—Same as Fig. 4 but for $\alpha = 2.5$

different values of the spectral index α (see also Fig. 2). It is seen that, though the average energy and filling factor are about the same in both cases, their variability is quite different. Since the average energy of nanoflares, given by equation (20), for $\alpha = 2.5$ is twice that for $\alpha = 4$, the average number of heating events providing the same energy flux q is, respectively, twice as small, so fluctuations are more strongly pronounced (see also Kopp & Poletto 1993). Obviously, a similar effect can be achieved by reducing $(\Delta W)_{\min}$ while keeping α fixed.

Observationally transient brightenings are detected as fluctuations in the loop emission, but existing information about the intensity spectrum of these fluctuations is quite controversial. Some observations (Krucker & Benz 1998; Parnell & Jupp 2000) report a power law with the spectral index greater than 2, while earlier data (Shimizu 1995) show a spectral index less than 2, thus casting doubt in the entire concept of the nanoflare heating. Therefore, understanding how nanoflare heating with the energy spectrum as described in equation (18) translates into loop emission variability is an important issue. Such a study, using the model described above, is presently underway. Preliminary results show that correspondence between the two spectra is not just a simple mirroring. The calculated spectrum of transient brightening typically consists of two different power-law domains. For large intensities the spectral index is close to that of nanoflares, as these fluctuations are caused by individual heating events with high energy $[\Delta W \gg (\Delta W)_{\min}]$. However, at lower intensities the spectrum is more flat because it results from interference of several nanoflares. It is, therefore, tempting to speculate that the difference in observed spectra of transient brightening is just a reflection of these two slopes within a single spectrum.

The support and hospitality of the National Astronomical Observatory of Japan, where this study was undertaken during the visit of one of the authors (G. V.), are gratefully acknowledged. This work was also supported by the UK Particle Physics and Astronomy Research Council and the British Council (G. V.). We thank S. Tsuneta for stimulating discussions.

REFERENCES

Antiochos, S. K., & Sturrock, P. A. 1978, ApJ, 220, 1137
Cargill, P. J. 1993, Sol. Phys., 147, 263
———. 1994, ApJ, 422, 381
Cargill, P. J., & Klimchuk, J. A. 1997, ApJ, 478, 799
Cargill, P. J., Mariska, J. T., & Antiochos, S. K. 1995, ApJ, 439, 1034
Galeev, A. A., & Sagdeev, R. Z. 1984, in Handbook of Plasma Physics, ed. M. N. Rosenbluth & R. Z. Sagdeev (New York: North Holland), chap. 6.1
Golub, L., Maxson, C., Rosner, R., Vaiana, G. S., & Serio, S. 1980, ApJ, 238, 343
Kopp, R. A., & Poletto, G. 1993, ApJ, 418, 496
Krucker, S., & Benz, A. O. 1998, ApJ, 501, L213
Low, B. C., & Wolfson, R. 1988, ApJ, 324, 574
Moore, R. L., Falconer, D. A., Porter, J. G., & Suess, S. T. 1999, ApJ, 526, 505
Parker, E. N. 1972, ApJ, 174, 499
———. 1988, ApJ, 330, 474
Parnell, C. E., & Jupp, P. E. 2000, ApJ, 529, 554
Priest, E. R. 1982, Solar Magnetohydrodynamics (Dordrecht: Reidel)
Rosner, R., Tucker, W. H., & Vaiana, G. S. 1978, ApJ, 220, 643

Serio, S., Reale, F., Jakimiec, J., Sylwester, B., & Sylwester, J. 1991, A&A, 241, 197
Shimizu, T. 1995, PASJ, 47, 251
Shimizu, T., & Tsuneta, S. 1997, ApJ, 486, 1045
Ulmschneider, P., Rosner, R., & Priest, E. R. 1991, Mechanisms of Chromospheric and Coronal Heating (Berlin: Springer-Verlag)
Van Ballegooijen, A. A. 1988, Geophys. Astrophys. Fluid Dyn., 41, 181
Vekstein, G. 1996, in Magnetodynamic Phenomena in the Solar Atmosphere (Dordrecht: Kluwer), 29
Vekstein, G., & Jain, R. 1998, Phys. Plasmas, 5, 1506
———. 1999, Phys. Plasmas, 6, 2897
Vekstein, G., Priest, E. R., & Amari, T. 1991, A&A, 243, 492